CLM-P548

CLM-P548

UKAEA

Preprint

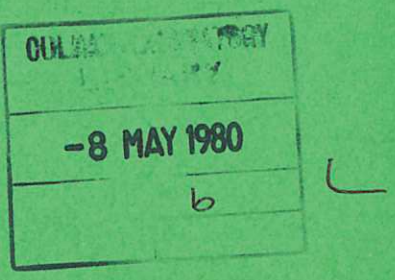

SIGNAL-TO-NOISE REQUIREMENTS FOR INTERPRETING SUBMILLIMETRE LASER SCATTERING EXPERIMENTS IN A TOKAMAK PLASMA

L. E. SHARP
A. D. SANDERSON
D. E. EVANS

CULHAM LABORATORY
Abingdon Oxfordshire

1980

CLM-P548

SIGNAL-TO-NOISE REQUIREMENTS FOR INTERPRETING SUBMILLIMETRE LASER SCATTERING EXPERIMENTS IN A TOKAMAK PLASMA

L E Sharp* A D Sanderson and D E Evans

UKAEA Culham Laboratory (EURATOM/UKAEA Fusion Association)
Abingdon, Oxon OX14 3DB, England

ABSTRACT

A Monte Carlo technique has been used to generate numerical simulations of the collective spectra of laser radiation scattered by plasma as they would be measured in a heterodyne receiver. Plasmas having ion temperatures in the range 500-5000 eV, contaminated by up to 2% fully stripped oxygen were investigated. The receiver output signal-to-noise ratio S required to measure T_i to better than 15% by a chi-square curve fitting procedure was found to be about 6 but even poor estimates of impurity concentration demanded much higher values of S . Since signal-to-noise ratios at the input and the output of the heterodyne receiver are almost independent when the former exceeds one, only the width of the resolution intervals and the integration time (laser pulse length) exert an appreciable influence on S , and optimum values for these parameters are investigated.

(Submitted for publication in Plasma Physics)

*Research School of Physical Sciences, Australian National University, Canberra, Australia

February 1980

1. Introduction

It is widely recognized [1] that measurement of ion temperature near the centre of tokamak plasmas using conventional techniques such as those based on charge exchange collisions will encounter serious difficulties in the new generation of plasma machines, whose large dimensions will prevent the escape of neutrals formed in the central region. As a consequence, interest has grown in an alternative approach based on scattering submillimetre or far infrared (FIR) wavelength electromagnetic radiation from collective density fluctuations in these plasmas [2]. The frequency spectrum of radiation collectively scattered by a plasma, which is measured when the scattering scale length exceeds the plasma Debye length, conveys spatially resolved information bearing on the ion and electron temperatures [3], impurities and effective charge [4], magnetic field [5] , and the level of microturbulence [6].

This paper deals with an aspect of the feasibility of performing a FIR scattering experiment on a typical tokamak discharge, which seems to have been ignored. We calculate the minimum measurement accuracy required to interpret the resulting frequency spectrum. For this purpose a Monte Carlo technique has been employed to simulate numerically the scattered light spectrum as it might be measured in a real experiment. Then the signal-to-noise ratio required to allow T_i and impurity concentration to be determined to any desired degree of accuracy has been derived using a chi-square test to find the best fit between simulated spectra and theoretical distributions.

2. Theory of Scattering

A well collimated monochromatic beam, wave vector $\underline{k}_o$, illuminates a plasma, and radiation scattered at angle θ with wave vector $\underline{k}_s$ reaches the detector. The wave vectors $\underline{k}_o$ and $\underline{k}_s$ determine the spatial Fourier component of the plasma electron density fluctuation, namely that for which $\underline{k} = \underline{k}_s - \underline{k}_o$, whose frequency spectrum will be measured. The scattered intensity on the detector will be

$$I(\underline{k},\omega) = I_o \frac{d\sigma}{d\Omega} n_e \Omega S(\underline{k},\omega) V \qquad ...(1)$$

where I_o is the power per unit area incident on the scattering volume V , $\frac{d\sigma}{d\Omega} = 7.9 \times 10^{-26}$ cm^2 is the Thomson differential cross-section for incident radiation polarized normal to the plane of scattering, n_e is the average electron density, Ω is the solid angle subtended by the collection optics at the scattering volume, and $S(\underline{k},\omega)$ is the dynamic form factor. The latter, related to the electron density auto-correlation by the Wiener-Khinchin theorem, has been calculated by various authors [7] for plasmas near thermal equilibrium.

For a plasma containing several ion species the form factor can be written in terms of G_e and G_j , the dielectric susceptibilities of the electrons and of the ions of species j ,

$$S(\underline{k},\omega) = \frac{\left|1 - \Sigma_j G_j\right|^2 F_e + \left|G_e\right|^2 n_e^{-1} \Sigma_j Z_j^2 N_j F_j}{\left|1 - G_e - \Sigma_j G_j\right|^2} . \qquad ...(2)$$

F_e and F_j are the velocity distributions, assumed to be Maxwellian, of electrons and of ions of species j , N_j is the number density of ions of type j, and Z_j is their charge.

The dielectric susceptibilities are related to the plasma dispersion function [8]

$$W(x) = 1 - 2xe^{-x^2}\int_0^x e^{t^2}dt - i\sqrt{\pi}\, xe^{-x^2}$$

with $x = \frac{\omega}{k\,v}$, v being the thermal velocity $\sqrt{\frac{2KT}{m}}$, by

$$G_e = -W\alpha^2 \quad \text{and} \quad G_j = -Z_j\frac{T_e}{T_j} W\,\alpha^2$$

where α is the usual scale length to Debye length ratio.

Upon inspection, the form factor is found to consist of a wide low intensity part coming from the first term in equation (2), and a tall narrow part coming from the second term. The latter stems from the collective motion of the electrons with the ions, which is what we are concerned to measure, so calculations have been confined to values of angular frequency ω for which this term makes a substantial contribution to the whole spectrum, i.e. $\omega \lesssim 3\,k\,v_i$.

Although tokamak plasmas can contain a number of different impurity species [9], we have assumed a hydrogen plasma contaminated by only 2% fully stripped oxygen (Z=8) as an acceptable model for the plasma in the central region of a typical tokamak [10].

In a real experiment measurable spectral width is constrained to lie within the bandwidth capability of the heterodyne detector and conventional electronics, typically less than 1 GHz. Since spectral width for equal T_e and T_j is given by

$$\Delta\nu \equiv \frac{kv_i}{2\pi} = \frac{\sqrt{2}\,\omega_{pi}}{2\pi\,\alpha} ,$$

this condition can easily be met by working at sufficiently high α . However, the danger that turbulence will overwhelm thermal fluctuations is least at low α . It can be seen that for a deuterium plasma having ion density in the range

$10^{13} - 10^{14}$ cm^{-3}, a value of $\alpha \sim 3$, which gives spectral widths less than 1 GHz, may be a satisfactory, indeed necessary compromise.

3. Heterodyne Detection and Signal-to-Noise Ratios

The theory of heterodyne detection [11] shows that when a weak radiation field having its intensity distributed over frequency according to the function $I_s(\nu)$, and a strong local oscillator at a fixed unique frequency $\nu_{\ell o}$ are superimposed on a square law detector, the resulting detector current i_1 has a power spectrum $P_1(\nu)$ given by (ref 11, equation 2.19)

$$P_1(\nu) = e\, i_{\ell o} + 2\pi\, i_{\ell o}^2 \delta(\nu) + i_{\ell o} \langle i_s \rangle \int_{-\infty}^{\infty} [e^{2\pi i(\nu+\nu_{\ell o})\tau} g_s^{(1)}(\tau) + e^{2\pi i(\nu-\nu_{\ell o})\tau} g_s^{(1)}(\tau)^*]\, d\tau .$$

In this expression $g_s^{(1)}(\tau)$ is the normalized first order auto-correlation function of the weak radiation field, defined by

$$g_s^{(1)}(\tau) \equiv \frac{\langle E_s^*(t) E_s(t+\tau) \rangle}{\langle E_s(t)^2 \rangle} = \frac{e\eta}{h\nu}\, \varepsilon_o c\, \frac{\langle E_s^*(t) E_s(t+\tau) \rangle}{\langle i_s \rangle}$$

since $\langle i(t) \rangle = \frac{e\eta}{h\nu} \langle I(t) \rangle = \frac{e\eta}{h\nu}\, \varepsilon_o c \langle E(t)^2 \rangle$.

Here, i_s is the detector current due to the weak radiation alone, $E(t)$ is radiation electric field, η is "quantum efficiency", and the other symbols have their usual meanings. Substituting $g_s^{(1)}(\tau)$ into the integral term of $P_1(\nu)$, and dropping the first part of the integrand which leads, for us, to a physically unobservable contribution, yields

$$i_{\ell o} \frac{e\eta}{h\nu}\, \varepsilon_o c \int_{-\infty}^{\infty} e^{2\pi i(\nu-\nu_{\ell o})\tau} \langle E_s^*(t)\, E_s(t+\tau) \rangle^*\, d\tau$$

which $= i_{\ell o} \frac{e\eta}{h\nu} [\, I_s(\nu-\nu_{\ell o}) + I_n(\nu-\nu_{\ell o})\,]$

by the Wiener-Khinchin theorem. The weak field power spectrum at the beat frequency $\nu-\nu_{\ell o}$ has been divided into two parts $I_s + I_n$, the former being signal and the latter optical background, e.g. plasma radiation. Then the heterodyne spectrum can be written

$$P_1(\nu) = e\, i_{\ell o} + 2\pi i_{\ell o}{}^2 \delta(\nu) + i_{\ell o}\frac{e\eta}{h\nu}[I_s(\nu-\nu_{\ell o})+I_n(\nu-\nu_{\ell o})]. \quad ...(3)$$

The first term above represents shot noise, the second, of which a factor is the Dirac delta function $\delta(\nu)$, is accordingly absent except at zero frequency, and the third is the heterodyne spectrum. The latter can be seen to be an exact replica of the optical spectrum, but centred at a frequency equal to the difference between the weak radiation field and local oscillator frequencies. It is this power spectrum that one seeks to measure.

The signal-to-noise ratio at the detector can be written, using equation (3), as

$$s = \frac{\text{signal}}{\text{noise}} = \frac{i_{\ell o}\, {}^{e\eta}/_{h\nu}\, I_s(\nu-\nu_{\ell o})}{e i_{\ell o} + i_{\ell o}\, {}^{e\eta}/_{h\nu} I_n(\nu-\nu_{\ell o})} = \frac{I_s(\nu-\nu_{\ell o})}{\frac{h\nu}{\eta} + I_n(\nu-\nu_{\ell o})}. \quad ...(4)$$

It can be seen that in the absence of noise from either background or amplifier, the value of the signal necessary to make $s = 1$, the detector noise equivalent power (NEP), is simply ${}^{h\nu}/_{\eta}$.

An electronic spectrum analyser, of which a rudimentary block diagram is shown in Figure 1, processes the detector current and produces an output current which is proportional to $P_1(\nu)$, the detector current power spectrum. It is this output current that one actually measures, and it is made up of a signal component and a noise component. To estimate the signal-to-noise ratio characterizing the output current and

to relate it to the input signal-to-noise ratio, given by equation (4), it is necessary to trace the current through the spectrum analyser, and the outcome depends on the initial assumptions about the statistical character of the noise and signal. For example if the noise at the input is wideband and random, but the input signal is coherent and sinusoidal, then the analysis of Smith [12] applies. If, as in our case, both signal and noise have wide bandwidth compared to that of the intermediate frequency filter (filter A in the diagram, Figure 1) then the treatment described by Cummins and Swinney [11] is appropriate. Here, signal and noise are indistinguishable, except by removing the optical signal from the radiation detector. Together, they constitute, statistically speaking, a random Gaussian process, which upon passing through the squaring element, becomes χ^2-distributed [13]. Moreover, the squarer mixes the noise and signal components in such a way that beyond it, noise in the presence of signal is different from noise when signal is absent.

Immediately following the squarer, the average current i_3 is proportional to the power P_1. The latter can be regarded as the sum of signal and noise parts: $P_1 = P_s + P_n$ when optical signal is falling on the detector, but $P_1 = P_n$ alone when optical signal is absent. Accordingly the desired signal at this stage, which will be proportional to the optical power, is

$$\langle i_3 \rangle_{s+n} - \langle i_3 \rangle_n \ .$$

A measure of the noise in the current at any stage is the root mean square fluctuation from the mean. In the case of i_3 this is

$$\sqrt{\langle (\Delta i_3)^2 \rangle} = \sqrt{(\langle i_3^2 \rangle - \langle i_3 \rangle^2)} \ .$$

The latter can be expressed either in the presence of signal

or in its absence. The signal-to-noise ratio for noise in the presence of signal gives a measure of the accuracy with which the signal is measured, while the signal-to-noise ratio in the absence of signal is a measure of the capacity of the system for detecting the expected signal against the prevailing noise background.

With these definitions, the signal-to-noise ratio for noise in the presence of signal at i_3 can be shown to be

$$\frac{s}{s+1} \quad \text{where} \quad s \equiv {}^{P_s}/_{P_n} \text{ is given by equation (4).}$$

That for noise in the absence of signal is simply s alone.

So at i_3 the signal-to-noise ratio for noise in the presence of signal is inevitably less than one, no matter how big s is. The integrator, filter B in the diagram, having time constant T, modifies this state of affairs, giving a final value for signal-to-noise ratio in the current i_4 of

$$\frac{\text{signal}}{\text{noise}}_{s+n} \equiv S = \frac{\langle i_4\rangle_{s+n} - \langle i_4\rangle_n}{\sqrt{(\langle i_4^2\rangle - \langle i_4\rangle^2)}\Big|_{s+n}} = \frac{s}{1+s}\sqrt{(1+\Delta\nu\, T)} \qquad \ldots(5)$$

where $\Delta\nu$ is the bandwidth of the resolution interval, filter A. At the same time we can define the detectability at i_4 as

$$D \equiv \frac{\langle i_4\rangle_{s+n} - \langle i_4\rangle_n}{\sqrt{(\langle i_4^2\rangle - \langle i_4\rangle^2)}\Big|_n} = s\sqrt{(1+\Delta\nu\, T)}\ .$$

These various quantities are illustrated in Figure 2.

Whereas the detectability D of the signal at the output of the frequency analyser is proportional to the signal-to-noise s at the optical detector, the output signal-to-noise S depends on s only if the latter is significantly smaller than one. If $s \gg 1$, $S \approx \sqrt{(1+\Delta\nu\, T)}$, and as such is independent of s. It is then determined exclusively by the parameters of the frequency analysing circuit.

The important conclusion for radiation scattering experiments when the spectrum is to be resolved by heterodyne detection followed by a conventional frequency analyser is that although detectability of the signal relative to the prevailing noise is proportional to the signal-to-noise ratio at the optical detector, no significant improvement in the signal-to-noise at the output can be effected by increasing the input signal-to-noise ratio.

The process of electrical integration that converts the mixer output current i_3 to the integrator output i_4 not only increases the signal-to-noise ratio, but also modifies the statistical distribution. A recipe for computing numbers belonging to the i_4 distribution can be derived based on the relation between $i_3(t)$ and $i_4(t)$, even though the latter itself is written only in the form of an integral.

Representing the electrical integrator network by its complex admittance

$$Y_B(\omega) = \frac{\Omega}{\Omega + i\omega} \quad , \quad \Omega \text{ being } = {}^{2\pi}/_{T} \quad ,$$

one can write $i_4(t)$ in terms of the corresponding unit impulse response [13] $y_B(t)$, the Fourier transform of $Y_B(\omega)$, operating on $i_3(t)$. That is

$$i_4(t) = \int_0^\infty i_3(t-\tau) y_B(\tau)\, d\tau = \int_0^\infty i_3(t-\tau)\, \Omega e^{-\Omega\tau}\, d\tau \, . \qquad \ldots(6)$$

Evidently the physical process of integrating $i_3(t)$ amounts mathematically to convolving it with a "window" function of the form $\Omega e^{-\Omega t}$.

Using equation (6) and the fact that $i_3(t)$ is χ^2-distributed, numbers belonging to the $i_4(t)$ statistical distribution can now be constructed numerically. It is likewise possible without knowing the $i_4(t)$ distribution explicitly, to demonstrate first that the averages of i_4 and i_3 are identical, viz

$$\langle i_4 \rangle = \langle i_3 \rangle ,$$

and second, that the signal-to-noise ratio at i_4 is $\sqrt{(1+\Delta\nu\ T)}$ times that at i_3.

4. Numerical Simulations

We imagine the frequency spectrum to be measured by an array of electrical spectrum analysers following the optical detector, of the kind illustrated schematically in Figure 1. Each spectrum analyser channel has an IF bandwidth $\Delta\nu$, and the whole array of channels spans the spectrum under investigation, $\Delta\nu$ playing the role of resolution interval.

To simulate a measured spectrum complete with noise, a theoretical distribution $S(\underline{k},\omega)$ (equation 2) is selected and divided into a set of channels each of width $\Delta\nu$. The average value of the theoretical curve in the qth channel, S_q, is treated as the mean of a χ^2-distribution for this channel, and a simulated experimental observation is constructed by forming the sum (the counterpart of the integral in equation 6)

$$[i_4]_q = \sum_{n=0} i_3(n)\ \frac{2\pi}{\Delta\nu\ T}\ e^{-n\ \frac{2\pi}{\Delta\nu\ T}} \qquad \ldots(7)$$

where $i_3(n)$ are numbers selected by a Monte Carlo technique from the χ^2-distribution

$$N(i_3) = \frac{e^{-i_3/\sigma^2}}{\sigma\sqrt{(\pi\ i_3)}}$$

with $\langle i_4 \rangle = \langle i_3 \rangle = \frac{\sigma^2}{2} = S_q$.

Provided the spectrum is truncated where the input signal-to-noise falls below one ($s < 1$), the value of signal-to-noise S can be taken to be the same in each channel. When this is the case, S in every channel is determined exclusively by the integration-bandwidth product $\Delta\nu\ T$, the latter being kept the same for each channel.

The resulting histogram, like that in Figure 3, is treated as though it were the result of a real measurement, and most likely values of ion temperature and impurity concentration are deduced by using a conventional chi-square fitting procedure to identify the theoretical spectrum that best fits this distribution.

As a practical exercise, collective ion features for hydrogen plasma contaminated by fully stripped oxygen were assumed, with electron density $n_e = 3 \times 10^{13}$ cm^{-3} (subject to increase by electrons from impurities), and impurity concentrations of 0.5%, 1.0%, and 2.0% by number. The range of electron temperature was T_e = 1, 2, and 3 keV, and ion temperature T_i = 0.5, 2.0, and 5.0 keV. The scale length to Debye length ratio α was 3 and 5, and the range of signal-to-noise S was taken as 2, 4, 6, and 10. Some results from these calculations are shown in TABLE I. Typical histograms calculated for S=6 are compared with best fit theory in Figure 4.

The calculations demonstrate that T_i can be measured with much greater accuracy than impurity concentration at a given signal-to-noise. TABLE II summarizes the average accuracies found for T_i and impurity level for different values of S, averaged over all cases. It shows that if T_i alone is required, then, for example, S=4 is adequate to ensure 25% accuracy, even though the impurity level will not be determined to better than about 60%.

At the levels of impurity under investigation, we find that oxygen contamination has no detectable influence on the accuracy with which T_i is determined.

The required value of S can be realized, according to equation (5), by an appropriate choice of resolution interval $\Delta\nu$ and of integration time T . It is worth reiterating that if scattered radiation is intense enough to make s>1, very

little further increase in S can be achieved by increasing the laser power to no matter what extent. Where a pulsed laser is used, integration time is limited to the laser pulse length. But since $\Delta\nu$ is also limited by the properties of detectors and ancillary electronics to a value $\lesssim$ 1 GHz, it will probably be obligatory to extend laser pulse lengths into the μsecond range to secure values of S necessary for reasonable accuracy in the T_i determination.

In choosing $\Delta\nu$ it can be seen that S suffers if the bandwidth is too small, but resolution is lost if $\Delta\nu$ is made too large. We investigated the importance of the number of resolution intervals by seeking the value of $\Delta\nu$ that minimized the uncertainty in the chi-square temperature estimate, for a fixed value of the integration time. Thus increasing the number of resolution intervals decreased S, and conversely. Results were rather inconclusive, but they appeared to indicate an improvement in T_i accuracy as the number of resolution intervals increased up to about 8, beyond which the indeterminacy in T_i grew once more.

Integration times,i.e. laser pulse lengths, required to obtain various output signal-to-noise values, assuming 10 resolution intervals of 10^8 Hz width are listed in TABLE II.

5. Experimental Design

In this section we consider briefly practical power requirements for a scattering experiment based on a pulsed FIR laser, by assuming collectively scattered radiation must exceed or at least equal the noise equivalent power (NEP) of the detector, and that it must also be much brighter than the plasma emission at the same frequency,i.e. $s \gtrsim 1$. An alternative approach, more suitable perhaps to the case of a CW laser, would be to seek conditions necessary to make output signal-to-noise $S>1$.

The best detector for heterodyne use near 0.5 mm wavelength is either the Schottky barrier diode [14], or the Josephson effect superconducting junction [15], both of which have NEP $\sim 3\times10^{-19}$ WHz^{-1} at this wavelength when used with appropriate local oscillators.

Radiation emitted by the plasma can obscure scattered light, and the black body value, into a heterodyne detector of etendu λ^2, I_{bb}= KT watts Hz^{-1} (K being Boltzmann's constant, T the temperature) may be expected to give the upper limit for emission from a plasma at any frequency. In the submillimetre range the brightest radiation emitted by a tokamak plasma is in the electron cyclotron harmonics (ECE). Costley [16] has computed ECE for JET conditions allowing for reflections on the torus walls, and finds $I_{ECE}\sim 3\times10^{-16}$ watts Hz^{-1} at λ = 0.5 mm, and $I_{ECE}\sim 2\times10^{-17}$ watts Hz^{-1} at λ = 385 μm, for T_e= 5 keV, n_e= 8×10^{13} electrons cm^{-3}, and B = 3 teslas. Using the approximate scaling $I_{ECE}\sim n_e B\, T_e^{m}$ where $m = \nu/\nu_{ce}$ is the harmonic number, I_{ECE} for other plasma conditions can be deduced from these figures. Thus one finds $I_{ECE}\sim 10^{-21}$ watts Hz^{-1} at 0.5 mm, and $I_{ECE}\sim 4\times10^{-24}$ watts Hz^{-1} at 385 μm for T_e= 1 keV, n_e= 3×10^{13} cm^{-3}, and B = 3 tesla. Evidently, whether ECE is larger or smaller than the detector NEP depends largely on the precise values of the plasma parameters, but for a wide range of parameters detector noise can be expected to dominate ECE.

Referring now to equations (1) and (4), we have that in some frequency interval the scattered power is

$$I(k,\omega)d\omega = I_o \frac{1}{\pi r^2} \frac{d\sigma}{d\Omega} n_e\, V\, \Omega\, S(k,\omega)\, d\omega > s[NEP] \frac{d\omega}{2\pi} \quad \ldots(8)$$

where I_o is the laser power which is focused down in the plasma onto area πr^2. V is the volume of plasma from which

scattered light is collected. The image of the collection aperture is assumed for convenience to have an area πr^2 too, so V is the volume common to two circular cylinders of the same radius r intersecting at an angle θ. Hence $V = \frac{16\ r^3}{3\sin\ \theta}$. The form factor can be approximated by its integral divided by its width, viz $S(k,\omega) \approx S_i(\alpha)/2\ k\ v_i$, where as usual, v_i is the projected ion thermal velocity.

Additionally, for heterodyning, the collection etendu is limited to λ^2 [17]: $\pi r^2 \Omega = \lambda^2$. The final condition is that in order to define k and hence temperature T_i, since $\frac{\Delta T}{T} = 2\ \frac{\Delta k}{k}$, a substantial number of scale lengths of the plasma fluctuation should be within the field of view [18]. In the arrangement described above, the number of wavelengths in view is $\zeta = \frac{4\ r}{\lambda} \tan \frac{\theta}{2}$, and accordingly, the laser power required, in the case of a deuterium plasma, is

$$I_o > 2.3\times10^{31}\ \frac{\zeta\sqrt{T_i}\ s[NEP]\ \sin\ \theta\ \cos\ \frac{\theta}{2}}{n_e\ \lambda^2\ S_i(\alpha)}\ \text{watts.} \quad ...(9)$$

The accompanying table, TABLE III, furnishes numerical examples for possible tokamak conditions, assuming deuterium plasma. It shows that for an experiment limited by detector noise at 3×10^{-19} watts Hz^{-1}, a laser power of about 0.1 MW at 0.5 mm secures a detection signal-to-noise s=1. Assuming window losses etc to introduce an additional factor of 10, the required laser power at 0.5 mm to measure T_i by collective scattering is about 1 MW.

6. Conclusions

The measurement of ion temperature by scattering sub-millimetre wavelength electromagnetic radiation from thermal fluctuations in a typical tokamak plasma free from strong microturbulence appears to be a practical possibility. Our detailed conclusions follow.

(1) Small scattering parameter α is desirable to minimize the effect of turbulence on the scattered spectrum. The smallest α consistent with a spectrum narrow enough to be handled by conventional detectors and electronics is $\alpha \sim 3$ in a plasma of typical tokamak density 10^{13}-10^{14} cm^{-3}.

(2) Assuming that heterodyne detector noise dominates, and that both signal and noise can be regarded statistically as wideband Gaussian processes, the signal-to-noise ratio at the detector is $s = I_s/[NEP]$, and at the output of the frequency analyser $S = \frac{s}{1+s}\sqrt{(1+\Delta\nu\ T)}$, where I_s is the intensity of the scattered radiation into the heterodyne detector per Hz bandwidth, $\Delta\nu$ is the bandwidth of the resolution interval, and T is the integration time, or pulse length in the case of a pulsed laser. Using these relations, numerical simulation of experimental data and chi-square fitting shows that ion temperature can be measured within 10's of percent accuracy if S exceeds about 2. If S=10, the accuracy can approach 10%. Estimates of impurity concentration are very much less accurate, however the presence of up to 2% fully stripped oxygen seems to have no adverse influence on the temperature measurement.

(3) Rather inconclusive computations suggest that best temperature accuracy is achieved if $\Delta\nu$ is chosen so that 6 to 8 resolution intervals span the beat frequency spectrum.

(4) It follows that since S depends only weakly on s when the latter exceeds one, and $\Delta\nu$ is effectively fixed by the choice of α and the need for optimum resolution, the values of

S required for the desired accuracy in T_i can be achieved only by increased laser pulse length T. Pulse lengths up to a few μseconds are indicated for S=10 for example.

(5) For signal-to-noise at detector of unity (s=1) in the presence of typical NEP= 3×10^{-19} watts Hz^{-1}, and making no allowance for systematic losses due to windows, beam transport, etc, a 0.5 mm FIR laser power of approximately 0.1 MW is required.

References

[1] TFR Group 6th IAEA Conference on Plasma Physics and Controlled Nuclear Fusion Research Berchtesgaden 1976 Paper CN35/A3
LA Berry, CE Bush, and JD Callen ibid. Paper CN35/A4/1

[2] FF Chen Comments on Plasma Physics and Controlled Fusion 1 81 (1972)
DL Jassby, DR Cohn, B Lax, and W Halverson Nuclear Fusion 14 745 (1974)
B Lax Proceedings of the 1st International Conference on Infrared Physics (CIRP I) Zurich (1975)

[3] DE Evans and J Katzenstein Reports on Progress in Physics 32 207 (1969)

[4] DE Evans Plasma Physics 12 573 (1970)
DE Evans and ML Yeoman Phys Rev Letters 33 76 (1974)
W Kasparek, H Hirsch, and E Holtzhauer to be published

[5] DE Evans and PG Carolan Phys Rev Letters 25 1605 (1970)
L Kellerer Zeitschrift fur Physik 239 147 (1970)
MJ Forrest, PG Carolan, and NJ Peacock Nature 271 718 (1978)

[6] MN Rosenbluth and N Rostoker Physics of Fluids 5 776 (1962)
CC Daughney, LS Holmes and JWM Paul Phys Rev Letters 25 497 (1970)
LE Sharp and S Mrowka J Physics D (Applied Physics) 8 2153 (1975)
RE Slusher, CM Surko, DR Moler and M Porkolab Phys Rev Letters 29 81 (1972)
CM Surko and RE Slusher Phys Rev Letters 37 1747 (1976)
RE Slusher and CM Surko Phys Rev Letters 40 400 (1978)
RE Slusher and CM Surko Physics of Fluids to be published

[7] JP Dougherty and DT Farley Proc Roy Soc A 259 79 (1960)
EE Salpeter Physical Review 120 1528 (1960)
T Hagfors J Geophysical Research 66 1699 (1961)

[8] BD Freid and SD Conte The Plasma Dispersion Function Academic Press (1961)

[9] TFR Group 3rd International Meeting on Theoretical and Experimental Aspects of Heating Toroidal Plasmas Grenoble 1976

[10] O Kluber Nuclear Fusion Letters 15 1194 (1975)

[11] HZ Cummins and HL Swinney Progress in Optics 8 135 (1970)

[12] RA Smith Inst of Electrical Engineers, Monograph No 6 (August 15, 1951)

[13] WB Davenport and WL Root Random Signals and Noise McGraw Hill (1958)

[14] JJ Gustincic Proc SPIE 105 Far Infrared and Submillimetre Waves 40-42 (1977)
A Semet, NC Luhmann, WA Peebles, G Morales, JJ Gustincic and Th de Grauuw 3rd International Conference on Submillimetre Waves and Their Applications Univ of Surrey England 1978 Paper FC2.3

[15] TG Blaney, NR Cross, and RG Jones 3rd International Conf on Submillimetre Waves and Their Applications Univ of Surrey, England 1978 Paper FC 1.11

[16] AE Costley P Brossier RJ Hastie
JET Workshop No4(2/75) Paper E23
Fontenay aux Roses 4/5 February 1975

[17] M Born and E Wolf Principles of Optics Pergamon 1959

[18] E Holzhauer and JH Massig Plasma Physics 20 867 (1978)

(a) $T_i = 0.5$ keV, $T_e = 1.0$ keV, $\alpha = 3$

$\frac{n_2}{n_1}$ =	2%		1%		0.5%	
S	T_i	$\frac{n_2}{n_1}$	T_i	$\frac{n_2}{n_1}$	T_i	$\frac{n_2}{n_1}$
2	625	1.21	371	7.6	228	5.63
4	430	1.95	551	0.68	526	0.38
6	527	0.85	589	0.82	456	0.98
10	496	3.13	548	0.63	504	0.60

(b) $T_i = 2.0$ keV, $T_e = 2.0$ keV, $\alpha = 3$

$\frac{n_2}{n_1}$ =	2%		1%		0.5%	
S	T_i	$\frac{n_2}{n_1}$	T_i	$\frac{n_2}{n_1}$	T_i	$\frac{n_2}{n_1}$
2	2326	1.89	1314	0.29	1479	0.03
4	2314	1.37	1592	1.31	1544	0.38
6	1776	2.29	2305	0.98	2073	0.76
10	2268	1.37	2496	0.78	1886	0.80

(c) $T_i = 5.0$ keV, $T_e = 3.0$ keV, $\alpha = 5$

$\frac{n_2}{n_1}$ =	2%		1%		0.5%	
S	T_i	$\frac{n_2}{n_1}$	T_i	$\frac{n_2}{n_1}$	T_i	$\frac{n_2}{n_1}$
2	2783	0.73	3791	0.38	1727	1.02
4	5755	0.30	4156	1.97	4103	0.74
6	4047	3.63	4145	1.80	5965	0.27
10	4245	2.60	5310	0.82	5752	0.23

Table I

Chi-square estimate of T_i, and fully stripped oxygen impurity concentration n_2/n_1 for a hydrogen plasma with $n_{eo} = 3 \times 10^{13}$ electrons cm^{-3}.

S	T (μsec)	T_i (%)	$\frac{n_2}{n_1}$ (%)
2	0.15	35	234
4	0.63	16	42
6	1.4	13	44
10	4.0	10	37

Table II

Summary of average percent uncertainty to be expected in T_i and impurity concentration measurements for the ranges of these parameters investigated, and for different values of the output signal-to-noise ratio S. T is the required integration time (pulse length) assuming resolution bandwidth $\Delta\upsilon$ = 100 MHz.

Given Parameters							Calculated Quantities				
$n_e(cm^{-3})$	$T_e(eV)$	$T_i(eV)$	$\lambda(\mu m)$	θ (°)	NEP (WHz^{-1})	$\frac{\Delta T_i}{T_i}$	I_o(MW)	α	$\Delta\nu$(MHz)	r(cm)	F-no.
$3\ 10^{13}$	$1\ 10^{3}$	$0.5\ 10^{3}$	385	30	$3\ 10^{-19}$	0.1	0.12	2.8	293	0.7	29
$3\ 10^{13}$	$3\ 10^{3}$	$5\ 10^{3}$	385	15	$3\ 10^{-19}$	0.1	0.10	3.2	468	1.5	60
$3\ 10^{13}$	$2\ 10^{3}$	$2\ 10^{3}$	385	20	$3\ 10^{-19}$	0.1	0.11	2.9	394	1.1	45
$3\ 10^{13}$	$1\ 10^{3}$	$1\ 10^{3}$	496	90	$3\ 10^{-18}$	0.2	0.85	1.3	880	0.1	4
$3\ 10^{13}$	$1\ 10^{3}$	$1\ 10^{3}$	496	90	$3\ 10^{-19}$	0.2	0.085	1.3	880	0.1	4
$1\ 10^{13}$	$3\ 10^{3}$	$5\ 10^{3}$	496	30	$3\ 10^{-19}$	0.1	0.74	1.2	720	0.9	29
$3\ 10^{13}$	$1\ 10^{3}$	$1\ 10^{3}$	114	30	$3\ 10^{-18}$	0.2	23.0	0.8	1400	0.1	15
$3\ 10^{13}$	$1\ 10^{3}$	$1\ 10^{3}$	114	15	$3\ 10^{-18}$	0.5	1.9	1.6	707	0.1	12

n_e electron density
T_e electron temperature
T_i ion temperature
λ laser wavelength
θ scattering angle
α Salpeter correlation parameter
I_o required laser power to make s=1
$\Delta\nu = k\ v_i/2\pi$ spectrum bandwidth
r radius of focal spot in plasma
F-no. Collection optics F-number

Table III

Numerical examples of possible tokamak conditions assuming deuterium plasma, showing laser power at wavelength λ required to make the input signal-to-noise s = 1.

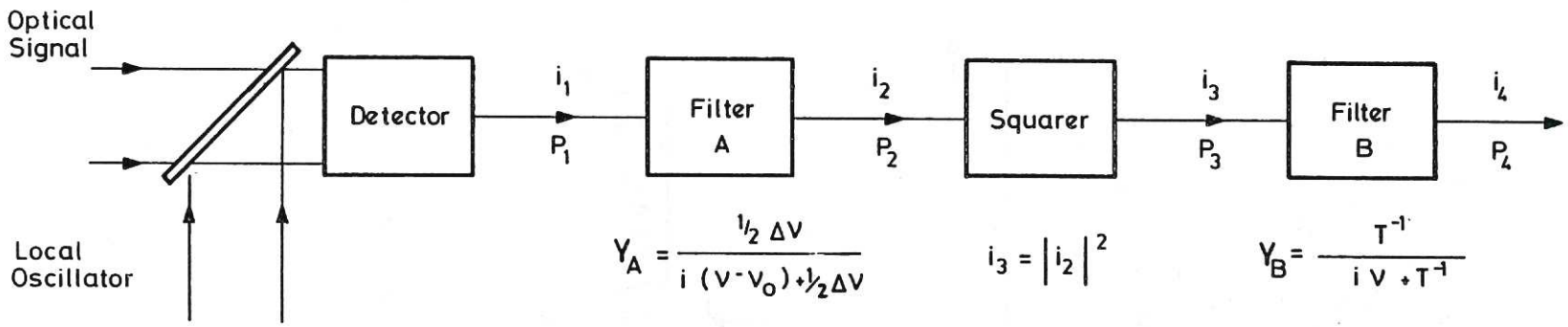

Fig.1 Block diagram of frequency analyser. Current at each stage is labelled i, power spectrum of current P. Filter A is the IF filter determining resolution bandwidth, and filter B is the integrator.

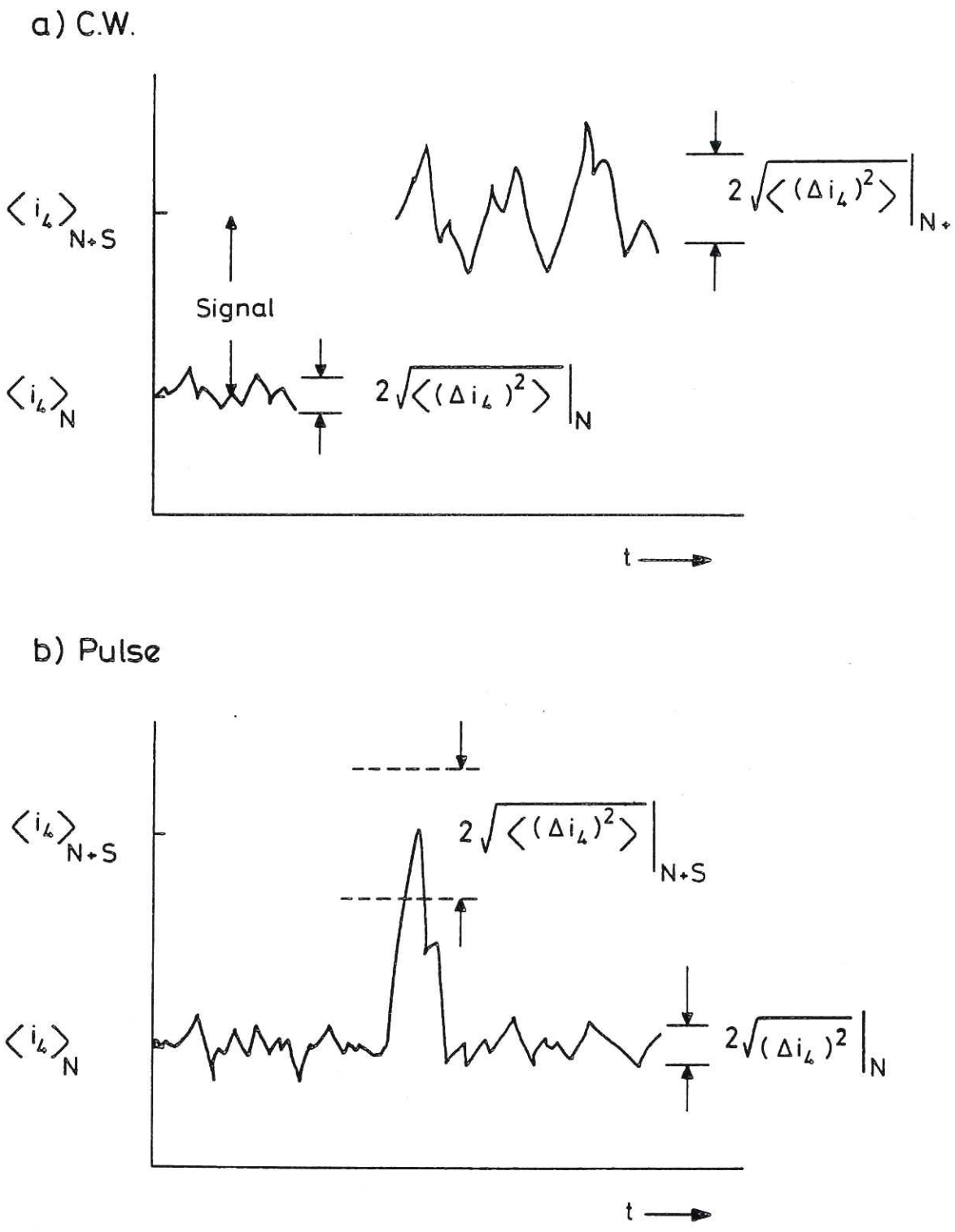

Fig.2 Output current i_4 from frequency analyser as a function of time, showing output in the absence of signal, and in its presence. (a) the continuous wave case and (b) the pulsed case.

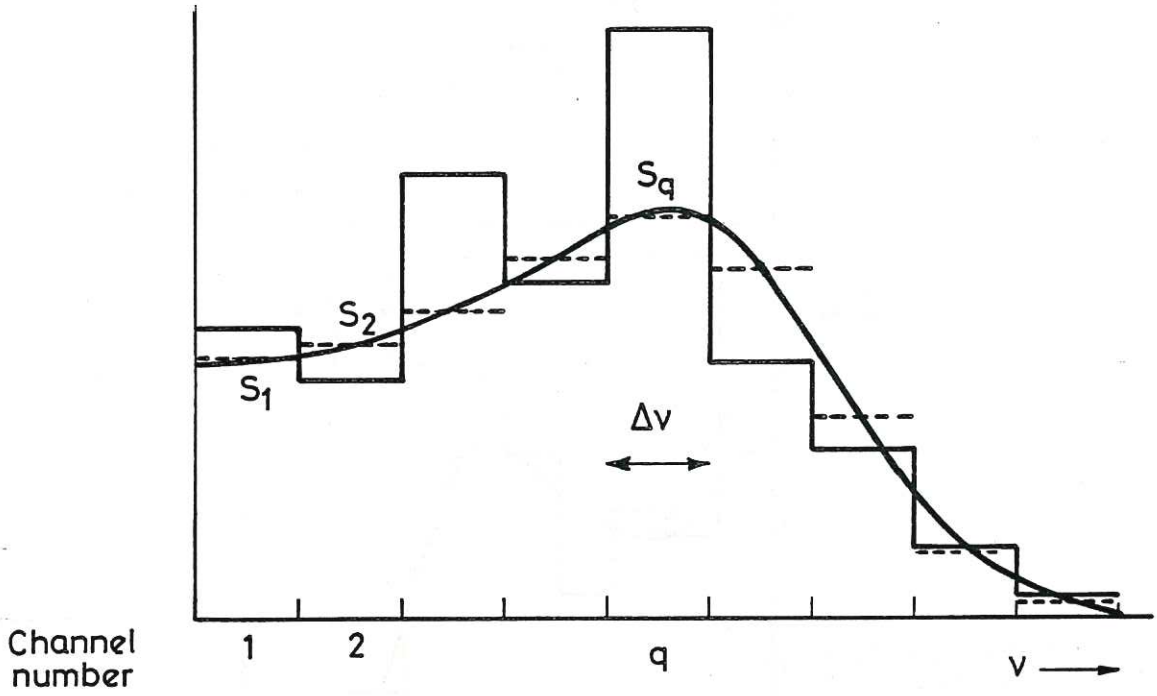

Fig.3 Example of a theoretical spectrum (solid curve) divided into a number of resolution intervals. Dotted line histogram is the average value of the theoretical curve in each channel. Solid line histogram is the simulated experimental result.

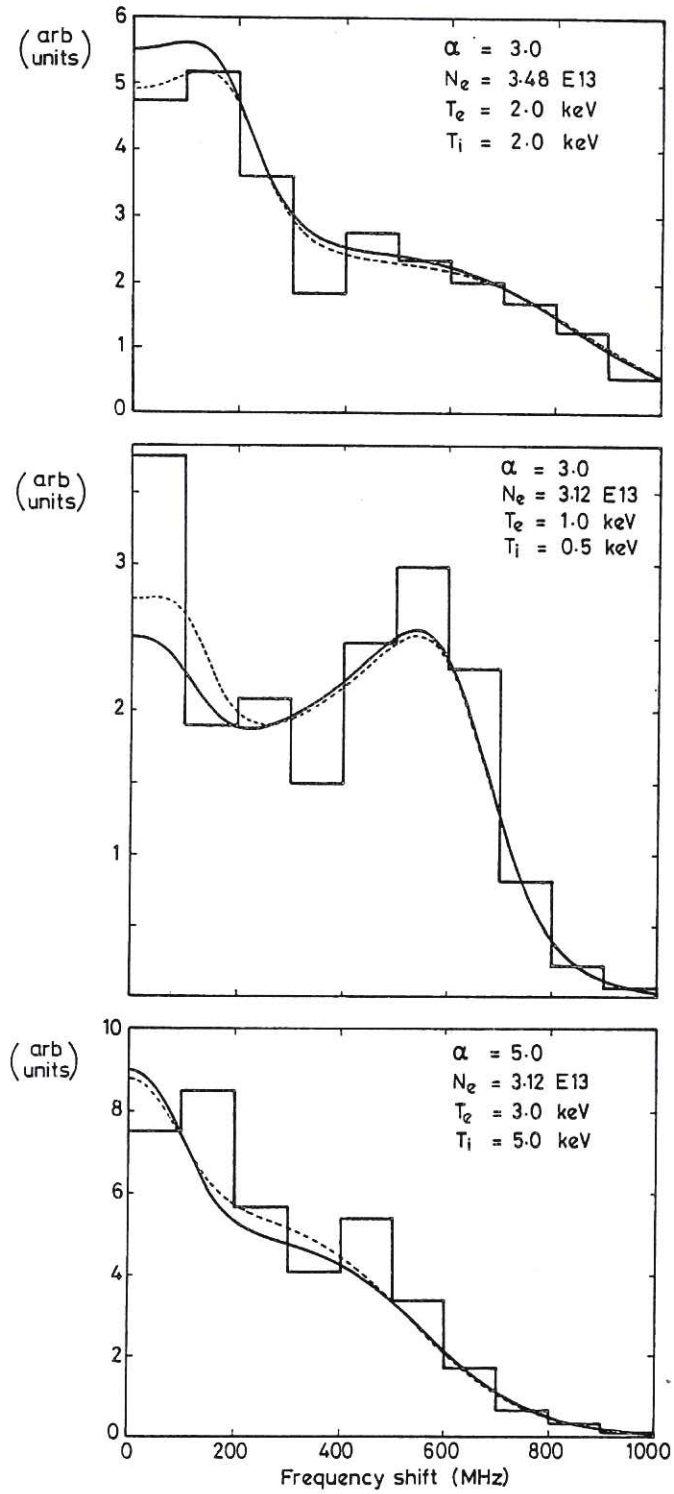

Fig.4 Examples of simulated experimental histograms constructed from theoretical spectra (solid curves) to which chi-squared best fits (dotted curves) have been assigned.

APPENDIX

In this appendix, we outline the calculation of the signal-to-noise ratio at the output of the frequency analyser following the approach indicated by Cummins and Swinney [11].

The frequency analyser circuit is sketched in Figure 1 where the IF filter A and the integrator B are each treated as having Lorentzian characteristics, that is, their complex admittances and their frequency spectra are given by

$$Y_A = \frac{\frac{1}{2}\,\Delta\omega}{i(\omega-\omega_o)+\frac{1}{2}\,\Delta\omega} \qquad |Y_A|^2 = \frac{(\frac{1}{2}\,\Delta\omega)^2}{(\omega-\omega_o)^2+(\frac{1}{2}\,\Delta\omega)^2} \qquad \ldots(A1)$$

$$Y_B = \frac{\Omega}{i\omega+\Omega} \qquad |Y_B|^2 = \frac{\Omega^2}{\omega^2+\Omega^2}$$

with $\Omega \equiv {}^{2\pi}/_{T}$, where T is the integration time.

It will prove helpful in what follows to recall that the Fourier transform of the Lorentz function

$$F(\omega) = \frac{a^2}{(\omega-\omega_o)^2 + a^2} \qquad \ldots(A2)$$

$$\text{is} \quad F(t) = \pi\, a\, e^{-at}\, e^{-i\omega_o t} \,.$$

The signal at the output of the frequency analyser will be

$$\langle i_4\rangle_{s+n} - \langle i_4\rangle_n \qquad \ldots(A3)$$

while the noise will be

$$\sqrt{\langle(\Delta i_4)^2\rangle} = \sqrt{(\langle i_4{}^2\rangle - \langle i_4\rangle^2)} \,. \qquad \ldots(A4)$$

Assuming that the spectrum $P_1(\omega)$ of the current i_1 is much broader than the passband of filter A,

$$P_2(\omega) = P_1(\omega_o) \left| Y_A \right|^2 . \qquad \ldots(A5)$$

We also require the autocorrelation function of the current

$$C(\tau) = \langle i^*(t)\, i(t+\tau) \rangle \qquad \ldots(A6)$$

which is related to the frequency spectrum by the Wiener-Khinchin theorem

$$P(\omega) = \frac{1}{2\pi} \int_{-\infty}^{+\infty} d\tau\, e^{i\omega\tau}\, C(\tau)$$

or inverting

$$C(\tau) = \int_{-\infty}^{+\infty} d\omega\, e^{-i\omega\tau}\, P(\omega) . \qquad \ldots(A7)$$

Accordingly, the current autocorrelation associated with $P_2(\omega)$ is

$$C_2(\tau) = \int_{-\infty}^{+\infty} d\omega\, e^{-i\omega\tau}\, P_1(\omega_o) \left| Y_A \right|^2$$

$$= P_1(\omega_o)\, \pi\, (\tfrac{1}{2}\, \Delta\omega)\, e^{-(\frac{1}{2}\, \Delta\omega)\tau}\, e^{-i\omega_o\tau}$$

by the use of equations A1 and A2. Since it can readily be seen that

$$C_2(0) = P_1(\omega_o)\, \pi\, (\tfrac{1}{2}\, \Delta\omega),$$

the foregoing autocorrelation function can conveniently be written

$$C_2(\tau) = C_2(0)\, e^{-(\frac{1}{2}\, \Delta\omega)\tau}\, e^{-i\omega_o\tau} . \qquad \ldots(A8)$$

Next, we assume that the operation of the squarer can be represented simply as

$$i_3(t) = \left| i_2(t) \right|^2 . \qquad \ldots(A9)$$

Thus the power spectrum of i_3 will be

$$P_3(\omega) = \frac{1}{2\pi} \int_{-\infty}^{+\infty} d\tau\, e^{i\omega\tau}\, C_3(\tau) = \frac{1}{2\pi} \int_{-\infty}^{+\infty} d\tau\, e^{i\omega\tau} \langle i_3(t) i_3(t+\tau) \rangle$$

$$= \frac{1}{2\pi} \int_{-\infty}^{+\infty} d\tau\, e^{i\omega\tau} \langle \left| i_2(t) \right|^2 \left| i_2(t+\tau) \right|^2 \rangle . \qquad \ldots(A10)$$

This integral is evaluated by introducing a theorem dealing with first and second order normalized autocorrelation functions $g^{(1)}(\tau)$ and $g^{(2)}(\tau)$ for random Gaussian variables. Where

$$C(\tau) = \langle i^*(t)\, i(t+\tau)\rangle = \langle |i(t)|^2\rangle\, g^{(1)}(\tau)$$

and $$\langle |i(t)|^2\, |i(t+\tau)|^2\rangle = \langle |i(t)|^2\rangle^2\, g^{(2)}(\tau) ,$$

it can be proved that [11]

$$g^{(2)}(\tau) = 1 + |g^{(1)}(\tau)|^2 ,$$

so $$\langle |i(t)|^2 |i(t+\tau)|^2\rangle = \langle |i(t)|^2\rangle^2 + |\langle i^*(t) i(t+\tau)\rangle|^2$$

$$= [C_2(0)]^2 + |C_2(\tau)|^2 . \qquad \ldots(A11)$$

Substituting this result into equation (A10) and using (A8) gives

$$P_3(\omega) = \frac{1}{2\pi}\int_{-\infty}^{+\infty} d\tau\, e^{i\omega\tau}\, [C_2(0)]^2 + \frac{1}{2\pi}\int_{-\infty}^{+\infty} d\tau\, e^{i\omega\tau}\, e^{-\Delta\omega\tau}\, [C_2(0)]^2$$

$$= [C_2(0)]^2 \left\{ \delta(\omega) + \frac{\Delta\omega/\pi}{\omega^2 + (\Delta\omega)^2} \right\} \qquad \ldots(A12)$$

using the definition of the δ-function, and the Fourier transform pair, equations (A2).

The current i_3 is integrated by filter B, leading to a power spectrum for i_4 given by

$$P_4(\omega) = |Y_B|^2\, P_3(\omega) \qquad \ldots(A13)$$

so $$\langle |i_4|^2\rangle \equiv C_4(0) = \int_{-\infty}^{+\infty} P_4(\omega)\, d\omega = \int_{-\infty}^{+\infty} d\omega\, \frac{\Omega^2}{\omega^2 + \Omega^2}\, P_3(\omega)$$

from equation (A1).

That is to say

$$\langle i_4^2 \rangle = \int_{-\infty}^{+\infty} d\omega \frac{\Omega^2}{\omega^2 + \Omega^2} [C_2(0)]^2 \left\{ \delta(\omega) + \frac{\Delta\omega/\pi}{\omega^2 + (\Delta\omega)^2} \right\}$$

$$\langle i_4^2 \rangle = [C_2(0)]^2 \left\{ 1 + \frac{1}{1 + \Delta\omega/\Omega} \right\} \qquad \ldots(A14)$$

where the integral $\int_{-\infty}^{+\infty} d\omega \frac{1}{(\omega^2 + \Omega^2)(\omega^2 + \Delta\omega^2)}$ was evaluated by the aid of the residue theorem.

We also require an expression for $\langle i_4 \rangle$ in order to construct the noise in i_4, given by equation (A4). We have

$$i_4(\omega) = Y_B(\omega)\, i_3(\omega)$$

and $i_3(\omega) = \frac{1}{2\pi} \int_{-\infty}^{+\infty} i_3(t)\, e^{i\omega t}\, dt = \frac{1}{2\pi} \int_{-\infty}^{+\infty} dt\, e^{i\omega t} |i_2(t)|^2$,

and at the same time

$$i_4(t) = \int_{-\infty}^{+\infty} i_4(\omega)\, e^{-i\omega t}\, d\omega .$$

So $\langle i_4(t) \rangle = \int_{-\infty}^{+\infty} i_4(\omega) \langle e^{-i\omega t} \rangle\, d\omega = \lim_{\tau \to \infty} \int_{-\infty}^{+\infty} d\omega \frac{\sin \omega\tau/2}{\omega\tau/2} i_4(\omega)$.

Substitute for $i_4(\omega)$ from the foregoing to obtain

$$\langle i_4(t) \rangle = \frac{1}{2\pi} \lim_{\tau \to \infty} \int_{-\infty}^{+\infty} |i_2(t)|^2 \left(\int_{-\infty}^{+\infty} Y_B(\omega)\, e^{i\omega t} \frac{\sin \omega\tau/2}{\omega\tau/2}\, d\omega \right) dt \qquad \ldots(A15)$$

Owing to the presence of $\frac{\sin \omega\tau/2}{\omega\tau/2}$ in the integral over ω, and the fact that τ approaches ∞, only very small values of ω contribute to the final value of the integral. Ignoring second order terms in ω therefore, the integral becomes

$$\int_{-\infty}^{+\infty} \frac{\sin \omega\tau/2}{\omega\tau/2}\, d\tau = \frac{2\pi}{\tau}$$

so that equation (A15) becomes

$$\langle i_4(t) \rangle = \lim_{\tau \to \infty} \frac{1}{\tau} \int_{-\infty}^{+\infty} |i_2(t)|^2\, dt \equiv \langle |i_2(t)|^2 \rangle \equiv C_2(0). \qquad \ldots(A16)$$

We are now in a position to construct the signal-to-noise ratio at the output of the frequency analyser. The noise part, equation (A4),

$$\sqrt{(\langle i_4^2\rangle - \langle i_4\rangle^2)} = \frac{C_2(0)}{\sqrt{(1 + \Delta\omega/\Omega)}}$$

from equations (A14) and (A16), while from equation (A16) the signal

$$\langle i_4\rangle_{s+n} - \langle i_4\rangle_n = [C_2(0)]_{s+n} - [C_2(0)]_n .$$

We recall that $C_2(0) = \frac{1}{2}\,\Delta\omega\,\pi\,P_1(\omega_o)$, where $P_1(\omega_o)$ is the spectrum of i_1 , that is, the optical spectrum, evaluated at the centre, ω_o, of the IF filter, filter A. When no optical signal falls on the detector, $P_1(\omega_o) \equiv P_n$, but when an optical signal is present, $P_1(\omega_o) \equiv P_n + P_s$, as can be seen by referring to equation 3 in the main body of the paper. Accordingly, signal-to-noise ratio when the noise is in the presence of signal is given by

$$S = \frac{[C_2(0)]_{s+n} - [C_2(0)]_n}{[C_2(0)]_{s+n}} \sqrt{(1 + \Delta\omega/\Omega)}$$

$$S = \frac{P_s + P_n - P_n}{P_s + P_n} \sqrt{(1 + \Delta\omega/\Omega)} = \frac{s}{s + 1} \sqrt{(1 + \Delta\omega/\Omega)} \qquad \ldots(A17)$$

where we have called $P_s/P_n \equiv s$.

The detectability, D, of the signal, which can be defined as the ratio of the signal to the noise-when-the-signal-is-absent, is given by

$$D \equiv \frac{[C_2(0)]_{s+n} - [C_2(0)]_n}{[C_2(0)]_n} \sqrt{(1 + \Delta\omega/\Omega)}$$

or

$$D = s\sqrt{(1 + \Delta\omega/\Omega)} . \qquad \ldots(A18)$$